Thermal sensors

SLEEPIR: Synchronized Low-Energy Electronically Chopped PIR Sensor for True Presence Detection

Libo Wu[1], Fangwang Gou[2], Shin-Tson Wu[2], and Ya Wang[1]

[1]*Department of Mechanical Engineering, Texas A&M University, College Station, TX 77843 USA*
[2]*CREOL, College of Optics and Photonics, University of Central Florida, Orlando, FL 32816 USA*

Manuscript received February 5, 2020; revised February 22, 2020; accepted February 25, 2020. Date of publication February 27, 2020; date of current version March 17, 2020.

Abstract—Passive infrared (PIR) sensors are widely used in motion sensing and lighting control. However, stationary occupants always trigger false-negative detects of PIR sensors and result in uncomfortable lighting swings and short lifetime of electronic appliances. To address this issue, a synchronized low-energy electronically chopped PIR (SLEEPIR) sensor is developed in this letter for true presence detection, where a liquid crystal (LC) optical shutter is proposed to electrically chop signals received by the PIR sensor in the long-wave infrared (LWIR) region (8–12 μm), where human skin radiates the most. Utilizing the anisotropic absorption property of the LC material, the shutter shows high modulation with a low driving voltage ($V_{\rm rms} = 4.17$ V). Instead of using the mechanical shutters previously developed by our group that are driven by motors, the SLEEPIR sensor reduces the power consumption,weight, volume, and noise level by 90.5%, 83.8%, 82.6%, and 100%, respectively, while maintaining high sensitivity and reliability. Thanks to the high modulation of the LC shutter in the LWIR region, the experimental results show that the SLEEPIR sensor could detect stationary occupants with high accuracy within the range of 4.0 m and with a large field-of-view of 100°.

Index Terms—Thermal sensors, light modulation, liquid crystal (LC) infrared shutter, passive infrared (PIR) sensor, presence detection.

I. INTRODUCTION

Passive infrared (PIR) sensors are widely used for occupancy presence detection [1], [2], occupancy positioning [3], tracking [4], and identification [5], owing to their low cost, low energy consumption, large detection range, and high reliability. However, a major shortcoming of PIR sensors is that they are motion detectors and, therefore, cannot detect stationary. A survey shows that the average time spent every day on stationary or equivalent to stationary activities, such as sleeping, studying, and watching television, is 11.8 h per indoor occupant [6]. Despite their popularity, such frequent false-negative detections and inaccurate occupancy estimations challenge their application with fast-growing smart home appliances. Adding active optical shutters that change the intensity of the received IR radiation is an intuitive option [7]–[10]. The group has previously developed optical shutters driven by different mechanical structures to block the IR radiation received by PIR sensor [7]–[9]. However, these optical shutters require mechanical parts and raise concerns about reliability and additional power consumption, noise, volume, and weight.

In this regard, this letter reports a synchronized low-energy electronically chopped PIR sensor (SLEEPIR) that utilizes a liquid crystal (LC) electronic shutter to chop the signals received by the on-board PIR sensor. As shown in Fig. 1(a), the SLEEPIR consists of one analog PIR sensor, NaPiOn AMN24112, Panasonic, Inc., a lab-made LC shutter with associated driving circuitry and an Arduino nanomicrocontroller unit (MCU). The LC shutter exhibiting high modulation in the long-wave infrared (LWIR) region, where human skin radiates the most. When operating, the LC shutter will periodically modulate the radiation from stationary occupants and, thus, trigger a response from the on-board PIR sensor of the SLEEPIR. This way, SLEEPIR extends the function of the traditional PIR sensors toward stationary occupants detection with a barely noticeable addition of weight, size, and power consumption.

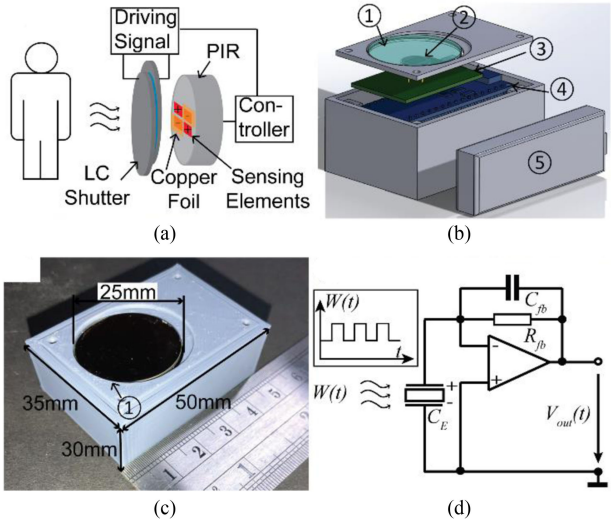

Fig. 1. (a) Schematic diagram of the SLEEPIR sensor. (b) Diagram of the prototype. (c) Photograph of the prototype with dimensions. (d) One pyroelectric sensing element receives the radiation *W(t)* followed by the preamplifier circuit. The inset demonstrates the periodical change of *W(t)*. ① LC shutter. ② PIR sensor. ③ Circuit board. ④ Microcontroller. ⑤ Battery.

II. DEVICE OVERVIEW

As shown in Fig. 1(b) and (c), the LC shutter fabricated in our lab consists of a high birefringence LC mixture, LCM-1660 (LC Matter, USA), sandwiched by two Germanium substrates. Unlike the

Corresponding author: Ya Wang (e-mail: ya.wang@tamu.edu).
Associate Editor: D. Utndani.
Digital Object Identifier 10.1109/LSENS.2020.2976801

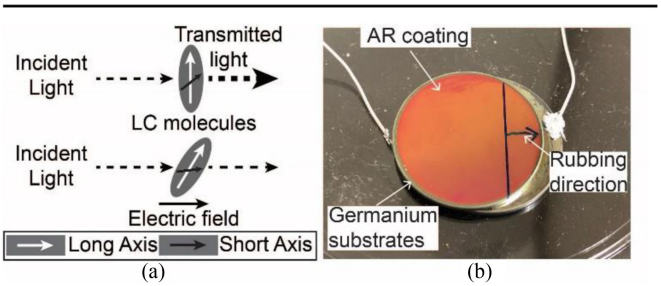

Fig. 2. (a) Working principle of the anisotropic absorption effect of the LC shutter. (b) Photograph of LC shutter.

traditional LWIR LC modulators reported in the literature [11]–[19], the LC shutter used in SLEEPIR exhibits a high transmittance, eliminates the use of polarizers and, therefore, significantly lowers the cost. As shown in Fig. 1(b), the driving circuit provides the ac signals at 122 Hz to turn the LC shutter ON and OFF at a period of 8 s. The MCU also receives the analog signal from the SLEEPIR, processes the data on the spot, and/or send it to the hub if there is a sensor network required. Note that the diagonal sensing elements of the PIR sensor are covered by copper foil to block IR signals in order to cancel the polarization in the opposite direction.

A. PIR Sensor Working Principle

As shown in Fig. 1(d), one pyroelectric sensing element, which is made of pyroelectric material, could convert the change of heat flux to current. When the radiation power received by the pyroelectric material is $W(t) = W_0\ e^{i\omega t}$, which is modulated at a frequency ω, then the voltage response $V_{\text{out}}\ (t)$ for the preamplifier stage is in the form of [20]

$$V_{\text{out}}\ (t) = \frac{R_{fb}\eta p' A\omega}{G_T\left(1+\omega^2\tau_T^2\right)^{1/2}\left(1+\omega^2\tau_E^2\right)^{1/2}} W\ (t). \tag{1}$$

Here, p' is the perpendicular component of the pyroelectric coefficient p; A is the area of the sensing element; η represents the emissivity of sensing element; $t_T = H/G_T$ and $\tau_E = R_{fb}\ C_{fb}$ represent the thermal and electrical constant, respectively, where H, G_T, R_{fb}, and C_{fb} stand for thermal capacity, thermal conductance, feedback resistance, and capacitance, respectively. Commercial-of-the-shelf PIR sensors normally consist of two or four sensing elements placed in series with opposite polarizations. By covering the sensing element(s) with the same polarization, the transmission change of the LC shutter would introduce obvious voltage signals from the PIR sensor, as shown in Fig. 1(a). When the LC shutter, which is in front of the PIR sensor, changes its transmission periodically, the received radiation $W(t)$ would change periodically, as shown in the inset of Fig. 1(d), thus causing the change of the output voltage $V_{\text{out}}\ (t)$.

B. LC Shutter Design and Property

In this letter, the LC shutter uses anisotropic absorption mechanism to modulate the IR light, as shown in Fig. 2(a). The LC compounds normally have a long axis and short axis. These two axes have different absorptions, depending on the incident light polarization. For an unpolarized input light, half of the intensity is along the long axis, and the other half is along the short axis. When no electric field is applied, the plane formed by the long and short axes is perpendicular to the incident light. Then, the light in both polarization directions encounters large absorption. As the electric field increases, the LC molecules will be reoriented along the longitudinal direction because the employed LCM-1660 has a positive dielectric anisotropy. In this case, the absorption of the long axis to the incident light that shares the same polarization direction decreases. Thus, the transmittance would increase. In other words, the electric field that applies to this kind of LC shutter would modulate the transmission rate. As aforementioned, this configuration does not require the use of polarizers and, thus, increases the overall transmittance and lowers the cost significantly.

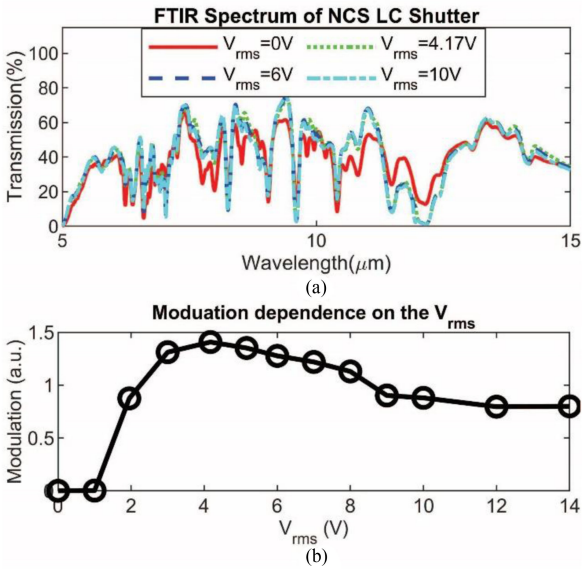

Fig. 3. (a) FTIR spectrums for various V_{rms} values. (b) Modulation over different V_{rms} in the range of 8–12 μm.

A commercial LC mixture, LCM-1660, which contains isothiocyanato (NCS) group, is chosen due to its high birefringence, large absorption anisotropy, low viscosity, and relatively large dipole moment [21].

To fabricate the LC shutter, the single-side antireflection-coated germanium (Ge) is chosen as the substrates due to its high transmission in the LWIR region and high conductivity. First, a thin polyimide layer is coated on the Ge substrates using spin coating. Then, alignment is created on the surface by rubbing. Two rubbed Ge substrates form an empty cell in an antiparallel way with 21 μm cell gap controlled by applying microsphere glass beads. Finally, LCM-1660 is injected into the empty cell due to the capillary effect. The photograph of the LC shutter is shown in Fig. 2(b).

The electro-optical property of the LC shutter is tested. The LC shutter is placed in the chamber of the Fourier-transform infrared spectroscopy (FTIR) (Thermo Scientific Nicolet iS5) spectrometer.

The external voltage is provided by a waveform generator (Keysight 33500B) and a voltage amplifier (Trek model 2220). The electric field is in the form of an alternating current square wave with the frequency of 100 Hz and various amplitudes. The V_{rms} of the applied ac voltage increases from 0 to 14 V. The FTIR spectrums in Fig. 3(a) show that the transmission rate of the LC shutter would change after the applied ac voltage. To quantify such changes, the modulation is defined as follows. First, we denote $T_{\text{ON}}(\lambda)$ and $T_{\text{OFF}}(\lambda)$ to be the transmission spectrum of the LC shutter with and without an applied voltage, respectively. In the remaining content, the states of the LC cell with or without an external voltage are referred to as ON-state and OFF-state, respectively.

According to Planck's law, a black body with the surface temperature T and the power emitted per unit area of the body, per unit solid angle of emission, and per unit wavelength λ is given by

$$B(\lambda) = \frac{2hc^2}{\lambda^5}\frac{1}{\exp\left(hc/\lambda k_B T\right) - 1} \tag{2}$$

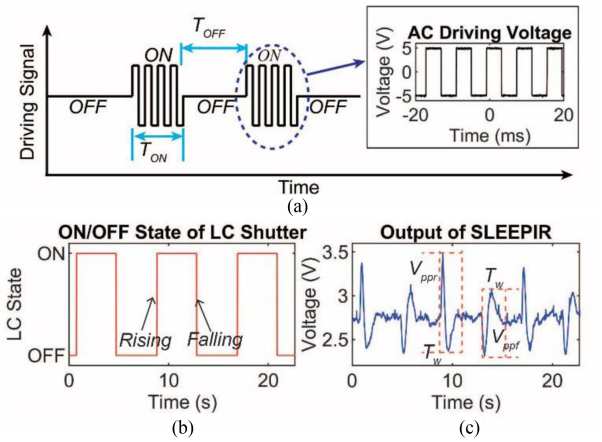

Fig. 4. (a) Driving signal that applies on the LC IR shutter. The blue circle indicates the ac voltage shown in the inset. (b) ON/OFF state of the LC shutter. (c) Output signal from the SLEEPIR sensor. The occupant is standing at a distance of 1.8 m with the angle of 0°.

where h is the Planck constant, c is the speed of light, and k_B is the Boltzmann constant. The emitted energy W_{ON} and W_{OFF} in the range of $[\lambda_1, \lambda_2]$ for both ON and OFF state could be written as

$$W_{\mathrm{ON}} = \int_{\lambda_1}^{\lambda_2} B(\lambda) T_{\mathrm{ON}}(\lambda)\, d\lambda, \quad W_{\mathrm{OFF}} = \int_{\lambda_1}^{\lambda_2} B(\lambda) T_{\mathrm{OFF}}(\lambda)\, d\lambda. \quad (3)$$

To simplify the modeling, we assume that the transition between the ON and OFF states follows the exponential equations, which are

$$W_{\mathrm{rise}}(t) = \frac{W_{\mathrm{ON}} - W_{\mathrm{OFF}}}{2} \exp(i\omega_r t) + \frac{W_{\mathrm{ON}} + W_{\mathrm{OFF}}}{2} \quad (4)$$

$$W_{\mathrm{fall}}(t) = \frac{W_{\mathrm{ON}} - W_{\mathrm{OFF}}}{2} \exp(-i\omega_f t) + \frac{W_{\mathrm{ON}} + W_{\mathrm{OFF}}}{2}. \quad (5)$$

Here, the subscripts rise and fall indicate the ON–OFF and OFF–ON transitions, respectively. The modulation frequencies ω_r and ω_f are related to the response time of the LC cell, $\omega_r = \pi/t_r$, $\omega_f = \pi/t_f$, where t_r and t_f represent the rise and decay time. By removing the dc component, (1) becomes

$$V_{\mathrm{out}} = \frac{R_{fb}\eta p' A_p \omega (W_{\mathrm{ON}} - W_{\mathrm{OFF}})}{2G_T (1 + \omega^2 \tau_T^2)^{\frac{1}{2}} (1 + \omega^2 \tau_E^2)^{\frac{1}{2}}} \quad (6)$$

where $\omega = \omega_r$ or ω_f for the rising or falling transitions, respectively. We define the term "modulation" as $W_{\mathrm{ON}} - W_{\mathrm{OFF}}$ with an arbitrary unit. Equation (6) shows that the response of a PIR sensor is proportional to the modulation. We calculate the modulation $W_{\mathrm{ON}} - W_{\mathrm{OFF}}$ in the range of $8 - 12\,\mu$m, and it is shown in Fig. 3(b). We surprisingly find that the maximum of the modulation happens when external voltage $V = 4.17\ V_{\mathrm{rms}}$. When $V > 4.17\ V_{\mathrm{rms}}$, the modulation starts decreasing. When $V > 12\ V_{\mathrm{rms}}$, the modulation saturates. Under such a high voltage, most of the LC directors have been reoriented by the electric field so that the optical modulation has reached the saturation level.

C. SLEEPIR Operation Method

From (6), the state of the LC shutter should change to introduce the output signal of the PIR sensor. To fulfill such operating conditions, the SLEEPIR sensor sends two channels of piecewise modulated signals in opposite phases to drive the LC shutter. Fig. 4(a) shows the driving ac voltage. The amplitude of the ac voltage is 4.9 V_{rms}. The time durations for ON and OFF states are T_{ON} and T_{OFF}, respectively. In this letter, $T_{\mathrm{ON}} = T_{\mathrm{OFF}} = 4$ s. The inset figure shows the actual field that applies to the LC shutter during ON state. Meanwhile, the MCU samples the analog signal from the PIR sensor at the frequency of 50 Hz. Table 1 presents some characteristics comparison of SLEEPIR and the chopped PIR sensors driven by the mechanical shutters developed by our group [6]–[8].

Table 1. Comparison Between SLEEPIR (This Letter), C-PIR [6], Ro-PIR [7], and LAMPIR [8].

Sensor	Weight (g)	Size (cm)	Power[a] (mW)	Sound level[b] (dBA)
C-PIR [6]	130.0	8.0×6.3×6.0	1050.0	42.6
Ro-PIR [7]	160.0	10.0×6.0×4.5	1680.0	36.0
LAMPIR [8]	40.0	6.5×4.30×4.5	190.0	30.2
SLEEPIR	21.0	3.0×3.50×5.0	100.0	0.0
Compare to C-PIR	-83.8%	-82.6%	-90.5%	-100.0%

[a]Power consumption includes the microcontroller and wireless module.
[b]Background sound level of acoustic sound level is 30.0 dB·A, measured using WENSN WS1361 sound level meter.

III. EXPERIMENTAL RESULTS

A. Test Setup

To characterize the SLEEPIR prototype for true human presence detection, the sensor node is placed facing front with a height of 1.0 m. One subject stands in front of the prototype. To measure the field-of-view (FOV), the SLEEPIR sensor node will rotate to different angles, while the subject remains in the same direction. The viewing angle increases from 0° to 50° with 10° increment. For each viewing angle, we first collect 1 min of data from the unoccupied scenario, then another 1 min of data when the subject is from 0.3 to 4.5 m away from the sensor with 0.3 m increment.

B. Presence Detection Result

One example waveform from the SLEEPIR sensor is plotted in Fig. 4(c) as well as the corresponding LC shutter state [see Fig. 4(b)]. The waveform is for the situation when the test subject stands stationary at 1.8 m away and the angle of the system is 0°. The SLEEPIR output shows polarity peaks whenever the state of the LC shutter changes, suggesting positive detection. The peaks at rising and falling edges of the LC states show the opposite phase since the transmission of the LC shutter changes oppositely. We define the peak-to-peak value V_{ppr} and V_{ppf} for the rising and falling transitions, respectively. They are calculated by subtracting the minimum value from the maximum value of the sensor signal within a window T_w. In this letter, we choose $T_w = 2$ s. The reason that V_{ppr} and V_{ppf} are different is that t_r and t_f of the LC shutter are different. Thus, the response voltage signal of the SLEEPIR sensor, which follows (6), would be different.

To differentiate the occupied and unoccupied scenarios, the maximum values of V_{ppr} and V_{ppf} for the unoccupied scenario are also plotted. More specifically, Fig. 5 shows the V_{ppr} values for each combination of viewing angle and occupant's distance. The threshold plane is chosen to be the maximum unoccupied V_{ppr} value, which is 0.5 V. The location whose V_{ppr} value is larger than the threshold value is classified as the occupied spot. The FOV and the detection range are also plotted in the inset of Fig. 5, indicating that the FOV of the SLEEPIR sensor is 100°, which is close to the onboard PIR

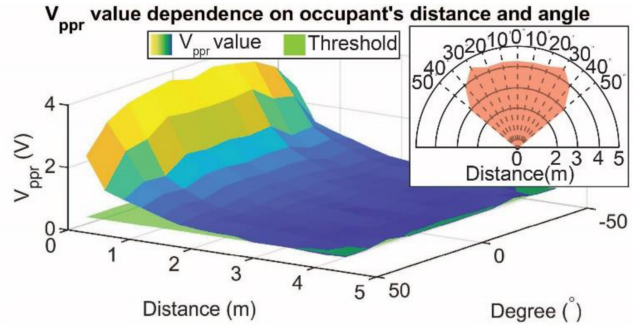

Fig. 5. Averaged V_{ppr} values when the occupant is at different distances and angles. The inset shows the corresponding FOV of the SLEEPIR sensor node.

sensor (100°). The experimental results reveal that the SLEEPIR sensor can detect stationary occupants in the range up to 3.0 m with the FOV of 100° at the accuracy of 100%.

IV. CONCLUSION

In summary, this letter reports a SLEEPIR for true human presence detection where an LC infrared electronic shutter with the associated facile driving circuit is proposed. Different from existing infrared optical shutters, the operation configuration builds off the LCM-1660 material that exhibits a high modulation in the LWIR region (8–12 μm). The configuration does not require high-cost IR polarizers or high driving voltage. The experimental results show that the SLEEPIR sensor can detect stationary occupants with 100% accuracy. The FOV of the SLEEPIR is found to be 100°, which is close to the onboard PIR sensor.

Future work will be focused on the following points:

1) improving the modulation of the LC shutter, including optimizing the cell gap of the LC shutter, and exploring other LC configurations;
2) decreasing the cost and power consumption of the proposed sensor node by exploiting the low-power modes of MCU;
3) conducting in-field experiments;
4) integrating machine learning methods so that statistical features extracted and ranked from the raw SLEEPIR output signal could be fed to machine learning models so that sensitivity can be further improved for field tests.

ACKNOWLEDGMENT

The work of TAMU Group was supported by the U.S. Department of Energy, Advanced Research Projects Agency-Energy, under Grant DE-AR0000945 and the work of UCF Group was supported by the Air Force Office of Scientific Research under Grant FA9550-14-1-0279.

REFERENCES

[1] T. A. Nguyen and M. Aiello, "Energy intelligent buildings based on user activity: A survey," *Energy Buildings*, vol. 56, pp. 244–257, Jan. 2013.
[2] M. Asif ul Haq *et al.*, "A review on lighting control technologies in commercial buildings, their performance and affecting factors," *Renewable Sustain. Energy Rev.*, vol. 33, pp. 268–279, May 2014.
[3] H. H. Kim, K. N. Ha, S. Lee, and K. C. Lee, "Resident location-recognition algorithm using a Bayesian classifier in the PIR sensor-based indoor location-aware system," *IEEE Trans. Syst., Man, Cybern, C Appl. Rev.*, vol. 39, no. 2, pp. 240–245, Mar. 2009.
[4] Q. Hao, F. Hu, and Y. Xiao, "Multiple human tracking and identification with wireless distributed pyroelectric sensor systems," *IEEE Syst. J.*, vol. 3, no. 4, pp. 428–439, Dec. 2009.
[5] J.-S. Fang, Q. Hao, D. J. Brady, B. D. Guenther, and K. Y. Hsu, "Real-time human identification using a pyroelectric infrared detector array and hidden Markov models," *Opt. Express*, vol. 14, no. 15, pp. 6643–6658, 2006.
[6] U.S. Bur. Labor Statist., U.S., Dept. Labor, *Amer. Time Use Surv.*, 2018. [Online]. Available: https://www.bls.gov/tus/home.htm, Accessed on: Mar. 9, 2020.
[7] H. Liu, Y. Wang, K. Wang, and H. Lin, "Turning a pyroelectric infrared motion sensor into a high-accuracy presence detector by using a narrow semi-transparent chopper," *Appl. Phys. Lett.*, vol. 111, no. 24, 2017, Art. no. 243901.
[8] L. Wu, Y. Wang, and H. Liu, "Occupancy detection and localization by monitoring nonlinear energy flow of a shuttered passive infrared sensor," *IEEE Sensors J.*, vol. 18, no. 21, pp. 8656–8666, Nov. 2018.
[9] L. Wu and Y. Wang, "A low-power electric-mechanical driving approach for true occupancy detection using a shuttered passive infrared sensor," *IEEE Sensors J.*, vol. 19, no. 1, pp. 47–57, Jan. 2019.
[10] C. F. Tsai and M.-S. Young, "Pyroelectric infrared sensor-based thermometer for monitoring indoor objects," *Rev. Sci. Instrum.*, vol. 74, no. 12, pp. 5267–5273, 2003.
[11] F. Peng, Y. Chen, S.-T. Wu, S. Tripathi, and R. J. Twieg, "Low loss liquid crystals for infrared applications," *Liq. Cryst.*, vol. 41, no. 11, pp. 1545–1552, 2014.
[12] S.-T. Wu, "Infrared properties of nematic liquid crystals: An overview," *Opt. Eng.*, vol. 26, no. 2, 1987, Art. no. 262120.
[13] S.-T. Wu, U. Efron, and L. D. Hess, "Infrared birefringence of liquid crystals," *Appl. Phys. Lett.*, vol. 44, no. 11, pp. 1033–1035, 1984.
[14] M. Sakata, Y. Hamada, K. Takeuchi, K. Shibata, and K. Kuroki, "Characteristics of a liquid crystal IR chopper for pyroelectric IR sensors," *Sensors Actuator A, Phys.*, vol. 40, no. 3, pp. 195–201, 1994.
[15] S. Brugioni and R. Meucci, "Liquid crystal twisted nematic light modulator for the infrared region," *J. Opt. A, Pure Appl. Opt.*, vol. 6, no. 1, pp. 6–9, 2003.
[16] J. Kobayashi, J. Kita, and K. Yoshino, "A light chopper for infrared detection utilizing ferroelectric liquid crystal," *Electron. Commun. Jpn. II, Electron.*, vol. 80, no. 2, pp. 88–97, 1997.
[17] K. Yoshino and M. Ozaki, "New electro-optic effect of microsecond response utilizing transient light scattering in ferroelectric liquid crystal," *Jpn. J. Appl. Phys.*, vol. 23, no. 6, pp. L385–L387, 1984.
[18] J. Kobayashi, J. Kita, and K. Yoshino, "Application of pyroelectric sensor and IR-chopper with ferroelectric liquid crystal for human detection," *IEEJ Trans. Sens. Micromach.*, vol. 117, no. 3, pp. 132–136, 1997.
[19] J. W. McCargar, R. Ondris-Crawford, and J. L. West, "Polymer dispersed liquid crystal infrared light shutter," *J. Electron. Imag.*, vol. 1, no. 1, pp. 22–29, 1992.
[20] R. W. Whatmore, "Pyroelectric devices and materials," *Rep. Prog. Phys.*, vol. 49, no. 12, pp. 1335–1386, 1986.
[21] S. Gauza, H. Wang, C.-H. Wen, S.-T. Wu, A. J. Seed, and R. Dabrowski, "High birefringence isothiocyanato tolane liquid crystals," *Jpn. J. Appl. Phys.*, vol. 42, no. 6A, pp. 3463–3466, 2003.